Chapter 8

Transport through negative-U molecules

8.1 Introduction

We have discussed in Chapter 1 that the coupling between electronic and vibrational degrees of freedom has two principal consequences: (i) The tunneling matrix elements get renormalized by a translation operator, which describes the shift between molecular potential surfaces for different charge states. (ii) Through the interaction between electrons and vibrations, the system gains energy, which causes a reduction of the charging energy $U \to U - 2\lambda^2\hbar\omega_0$, the polaron shift. In previous chapters, we have extensively studied the consequence (i) of the electron-phonon coupling, and we have established that the tunneling-induced phonon dynamics governed by Franck-Condon physics leads to striking effects beyond the emergence of vibrational sidebands in the current-voltage characteristics. In this chapter, we focus on the second important consequence (ii) of a large polaron shift, which can lead to a *negative* effective charging energy U.

In physics, the concept of negative-U centers was first pointed out more than three decades ago by Anderson [119], and is realized in many amorphous semiconductors. In chemistry, the scenario of negative-U molecules is known as "potential inversion" [120]. In cyclic voltammogram measurements, the negative charging energy is signalled by a favoring of the doubly ionized molecular state, i.e. negative-U molecules prefer a charging by two electrons instead of one. An important ingredient in realizing this scenario in molecular junctions may be a reduction of the true molecular charging energy by screening due to metallic electrodes [121] or an electrolytic environment [20].

In general, finite on-site interaction (of any sign) opens a new transport channel between molecule and leads. Namely, at finite U, *two* electrons can hop onto the molecule *simultaneously*. Yet, it is only for negative U that this process can dominate the transport. Indeed, negative U favors even electron occupation numbers of the molecule. At low temperatures, the degeneracy between two even-number charge states leads to the development of the charge-Kondo effect. In this case, virtual pair transitions assume the role of spin-flips [122] (responsible for the conventional spin-Kondo effect), and lead to the formation of Kondo correlations in the ground state. However, the fact that the relevant pseudospin degree of freedom is associated with charge, makes this Kondo state rather fragile. The underlying reason for this was elucidated by Iche and Zawadowski [82] and Haldane [83], who pointed out that for the charge-Kondo effect, any deviation from degeneracy acts as a Zeeman field

on the pseudospin and, thus, suppresses the Kondo correlations. This observation has drastic consequences for transport. For the conventional spin-Kondo effect, the low-temperature conductance eventually reaches the unitary value over a wide range of gate voltages. By contrast, for the charge-Kondo effect the unitary value is only achieved *precisely* at the resonance gate voltage. This fragility of the charge Kondo effect in transport through molecules with negative U was illustrated by several recent numerical simulations [123–125].

In this chapter, we first explore the transport dynamics in negative-U molecules outside the Kondo regime, by calculating the current-voltage characteristics and zero-frequency noise in Sections 8.2-8.5. A main result of our investigation is that negative U strongly affects the transport through a molecule even in the rate-equation regime at high temperatures, where Kondo correlations are irrelevant. We show that in this regime, negative U leads to a unique scenario for the passage of current through the molecule, which we study analytically at all gate voltages and biases. In Section 8.6, we establish a generalization of the particle-hole transformation by Iche and Zawadowski, suitable for the transport situation. This particle-hole/left-right transformation opens up the possibility of mapping the current in the negative-U model to the current in a conventional Anderson model with a local Zeeman field. We exploit this mapping in both possible ways: In Section 8.7, we deduce transport characteristics for the Anderson model from our previous negative-U results. Finally, in Sections 8.8-8.9 we turn to an analytical investigation of the charge-Kondo effect by utilizing results known from the conventional spin-Kondo effect.

8.2 Effective Hamiltonian

We start from the Anderson-Holstein Hamiltonian

$$H = H_{\rm mol} + H_{\rm leads} + H_{\rm T}, \tag{8.1}$$

see Eqs. (1.1)–(1.3). As described in Chapter 1, the electron-phonon coupling is eliminated by the Lang-Firsov transformation [41, 45, 71], which implies renormalizations of the tunneling Hamiltonian $t_a \to t_a e^{-\lambda(b^\dagger - b)}$, of the orbital energy $\varepsilon_d \to \varepsilon_d - \lambda^2\hbar\omega_0$, and of the charging energy $U \to U - 2\lambda^2\hbar\omega_0$. It is this last renormalization which opens the possibility of a negative effective charging energy. The underlying reason for this renormalization is that the energetic polaron shift is proportional to the excess charge of the molecule *squared* which is of the same form as the Coulomb charging energy. To be specific, we focus on temperatures and biases where only the vibrational ground state is populated. In this case, we obtain an effective Hamiltonian

$$H_{\rm eff} = \varepsilon_d n_d + U n_{d\uparrow} n_{d\downarrow} + H_{\rm leads} + H_{\rm T} \tag{8.2}$$

with negative effective charging energy U and Franck-Condon suppressed tunneling matrix elements $t_a \to t_a e^{-\lambda^2/2}$ (absorbed into the definition of t_a in the following).

As the single-particle energy ε_d is tuned by a gate voltage, the electron occupation n_d of the molecule switches from empty ($n_d = 0$) to doubly occupied ($n_d = 2$) at the resonant gate voltage defined by the condition $2\varepsilon_d + U = 0$.[1] Due to the negative U, single

[1] In the presence of additional orbitals, this remains true as long as $|U|$ is smaller than the level spacing.

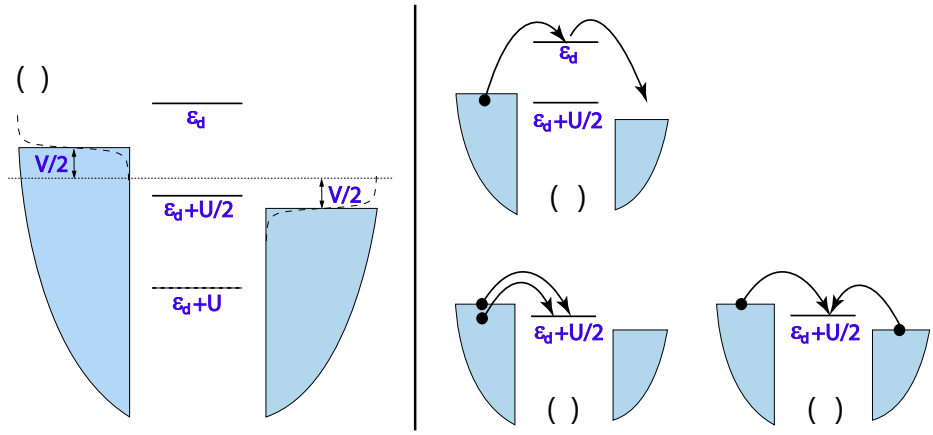

Figure 8.1: (a) Level configuration of the negative-U model. Shown are the one-particle energies for the singly-occupied molecule (ε_d), the doubly-occupied molecule ($\varepsilon_d+U/2$), and the energy for which holes can propagate through the doubly-occupied molecule (ε_d+U). The right panel illustrates the relevant types of processes: (b) cotunneling, (c) and (d) pair tunneling.

occupation ($n_d = 1$) of the molecule is unfavorable at any gate voltage. A schematic of the corresponding configuration of one-particle energies near resonance is shown in Fig. 8.1(a). Sequential tunneling of single electrons is clearly exponentially suppressed at bias voltages $|eV| \ll |U|$. Instead, the dominant sequential transport processes near resonance involve the coherent transfer of *electron pairs*.[2] Representative pair-tunneling processes are illustrated in Figs. 8.1(c) and (d). It is important to realize that in addition to processes in which the two electrons enter the molecule from the same lead, the electron pair on the molecule can be created (or annihilated) by two electrons tunneling in from (or out to) opposite leads. In parallel with these sequential pair-tunneling processes, single-particle cotunneling processes [see Fig. 8.1(b)] also take place. We find that while both processes are of the same order, they can be easily distinguished since the single-particle cotunneling contribution does not exhibit any structure near the resonance gate voltage.

To capture all eight pair-tunneling processes systematically, we perform a Schrieffer-Wolff transformation [126,127] (see Appendix A.2 for details). This eliminates the tunneling $H_{\rm T}$ to lowest order, and we obtain a transformed Hamiltonian

$$H_{\rm SW} = \varepsilon_d n_d + U n_{d\uparrow} n_{d\downarrow} + H_{\rm leads} + H_{\rm dir,ex} + H_{\rm pair}, \tag{8.3}$$

where we ignore a term which merely renormalizes ε_d. For positive U, one only retains

$$\begin{aligned} H_{\rm dir,ex} = & \frac{1}{2} \sum_{aa'\mathbf{p}\mathbf{p}'\sigma} \Bigg[\frac{t_a t_{a'}^*}{\epsilon_{a\mathbf{p}} - \varepsilon_d} c_{a\mathbf{p}\sigma}^\dagger c_{a'\mathbf{p}'\sigma} \\ & + t_a t_{a'}^* \, M(\epsilon_{a\mathbf{p}}) \left(d_{\bar\sigma}^\dagger d_\sigma c_{a\mathbf{p}\sigma}^\dagger c_{a'\mathbf{p}'\bar\sigma} - c_{a\mathbf{p}\sigma}^\dagger c_{a'\mathbf{p}'\sigma} n_{d\bar\sigma} \right) + \text{h.c.} \Bigg], \end{aligned} \tag{8.4}$$

[2] We define sequential-tunneling processes as involving real occupation of the molecule as opposed to cotunneling during which the molecule is only virtually occupied.

which describes the direct and exchange interactions between molecule and lead. Here, we have introduced the abbreviation

$$M(\epsilon) = \frac{1}{\epsilon - \varepsilon_d} - \frac{1}{\epsilon - (\varepsilon_d + U)}, \tag{8.5}$$

and we have denoted spin inversion by $\bar{\uparrow}, \bar{\downarrow} = \downarrow, \uparrow$. With $U > 0$ and in the absence of charge fluctuations, transport predominantly proceeds via single-electron cotunneling described by $H_{\rm dir,ex}$. By contrast, for negative U it is crucial to retain the pair-tunneling terms

$$H_{\rm pair} = \sum_{aa'\mathbf{p}\mathbf{p}'} t_a t_{a'}\, M(\epsilon_{a\mathbf{p}}) d_\uparrow d_\downarrow c^\dagger_{a'\mathbf{p}'\downarrow} c^\dagger_{a\mathbf{p}\uparrow} + \text{h.c.} \tag{8.6}$$

Obviously, $H_{\rm pair}$ contributes only for *nonzero* effective charging energy U.

8.3 Rates

Using Fermi's Golden Rule, the pair Hamiltonian $H_{\rm pair}$ leads to the rate

$$W^{aa'}_{0\to 2} = \frac{\Gamma_a \Gamma_{a'}}{h} \int d\epsilon\, M^2(\epsilon) f_a(\epsilon) f_{a'}(2\varepsilon_d + U - \epsilon), \tag{8.7}$$

for pairs of electrons tunneling onto the molecule.[3] Here, $\Gamma_a = 2\pi\rho_a |t_a|^2$ is the energy scale of single-particle tunneling in junction a for a constant density of states ρ_a. The superscripts (aa') denote the leads from where the spin-up electron (a) and the spin-down electron (a') originate. The analogous rates $W^{aa'}_{2\to 0}$ for pairs leaving the molecule are obtained from Eq. (8.7) by replacing each lead Fermi function f_a with a factor $(1 - f_a)$.

In the regime where single-particle occupation of the molecule is negligible, i.e.

$$|2\varepsilon_d + U|, |eV|, k_B T \ll \varepsilon_d,\ |\varepsilon_d + U|, \tag{8.8}$$

the integral in Eq. (8.7) approximately reduces to an integral over the Fermi functions alone, and can be expressed in terms of the function $F(\epsilon) = \epsilon/[\exp(\beta\epsilon) - 1]$. For symmetric voltage splitting,[4] i.e., $f_a(\epsilon) = f(\epsilon - eV_a)$ with $V_{L,R} = \pm V/2$, the explicit result for pair tunneling reads

$$W^{aa'}_{\rm x} = \frac{\Gamma_a \Gamma_{a'}}{h} M^2(0) F\left[\pm\left(2\varepsilon_d + U + eV_a + eV_{a'}\right)\right], \tag{8.9}$$

where the upper (lower) sign refers to $\mathrm{x} = 0 \to 2$ ($\mathrm{x} = 2 \to 0$). The pair-tunneling rates, Eq. (8.9), have several remarkable features.

(i) Pair tunneling with electrons originating from the same lead [$a = a'$, Fig. 8.1(c)] leads to bias-dependent rates. By contrast, pair tunneling with electrons from different leads [$a \neq a'$, Fig. 8.1(d)] is bias independent, as the energy missing in the lead with lower Fermi energy is exactly compensated for by the additional energy available in the lead with higher Fermi energy.

[3] We call attention to the fact that the notation for rates employed in this Chapter deviates from our usual notation.

[4] The generalization to asymmetric voltage splitting is straightforward.

(ii) When pair tunneling is energetically allowed, its rate is *proportional to the detuning* of the pair state $2\varepsilon_d + U$ from the relevant Fermi energy. This is in sharp contrast to rates for single-electron sequential tunneling, which are *independent* of the energy of the single-particle state.

This unusual behavior of the pair-tunneling rates arises from the fact that only the sum of the energies of the two tunneling electrons is fixed by energy conservation, making the *phase space* for pair tunneling proportional to the detuning.[5] We will see below that this leads to characteristic features of pair tunneling both in the gate-voltage and bias dependence of the conductance. Similarly, the rates for cotunneling from lead a to a' can be obtained from $H_{\rm dir,ex}$ as

$$W_{0\to 0}^{aa'} = 2\frac{\Gamma_a\Gamma_{a'}}{h}\frac{F(eV_a)}{\varepsilon_d^2}, \qquad W_{2\to 2}^{aa'} = 2\frac{\Gamma_a\Gamma_{a'}}{h}\frac{F(eV_a)}{(\varepsilon_d+U)^2}, \tag{8.10}$$

including an explicit factor of 2 for spin.

Having established the relevant processes and their rates, we now describe transport outside the Kondo regime by the corresponding rate equations [90,91]. Since the occupation probability for the singly-occupied molecule is negligible for $|eV| \ll |U|$, the stationary rate equations reduce to $0 = P_2W_{2\to 0} - P_0W_{0\to 2}$, with the solution $P_0 = W_{2\to 0}/[W_{2\to 0} + W_{0\to 2}]$, $P_2 = 1 - P_0$. Here, $W_{i\to f}$ denotes the total rate for transitions from initial state i to final state f, i.e., $W_{i\to f} = \sum_{a,a'} W_{i\to f}^{aa'}$. The stationary current $I = I^{\rm pairs} + I^{\rm cot}$, evaluated in the left junction, involves contributions from pair tunneling and cotunneling,

$$I^{\rm pairs}/e = P_0 w_{0\to 2} - P_2 w_{2\to 0}, \tag{8.11}$$

$$I^{\rm cot}/e = P_0 v_{0\to 0} + P_2 v_{2\to 2}. \tag{8.12}$$

Here, the coefficients v and w are given by

$$v_{0\to 0} = W_{0\to 0}^{LR} - W_{0\to 0}^{RL}, \quad w_{0\to 2} = 2W_{0\to 2}^{LL} + W_{0\to 2}^{LR} + W_{0\to 2}^{RL}. \tag{8.13}$$

The factor of 2 in the last equation originates from the coherent transfer of *two* electrons in this pair-tunneling process. [All remaining coefficients are obtained from Eq. (8.13) by interchanging "$2 \leftrightarrow 0$" in the subindices.]

8.4 Conductance and current-voltage characteristics

The rate equations provide a complete *analytical* description of the nonlinear current-voltage characteristics through negative-U molecules. Specifically, we find for the linear conductance

$$G = \frac{2e^2\Gamma_L\Gamma_R}{h}\left[\frac{U^2}{\varepsilon_d^2(\varepsilon_d+U)^2}\frac{\beta(2\varepsilon_d+U)}{2\sinh[\beta(2\varepsilon_d+U)]} + f(-2\varepsilon_d-U)\frac{1}{\varepsilon_d^2} + f(2\varepsilon_d+U)\frac{1}{(\varepsilon_d+U)^2}\right]. \tag{8.14}$$

[5] Similar phase-space arguments apply to pair tunneling between superconductors, see J. W. Wilkins, in *Tunneling Phenomena in Solids*, edited by E. Burstein and S. Lundqvist (Plenum Press, New York, 1969), chap. 24.

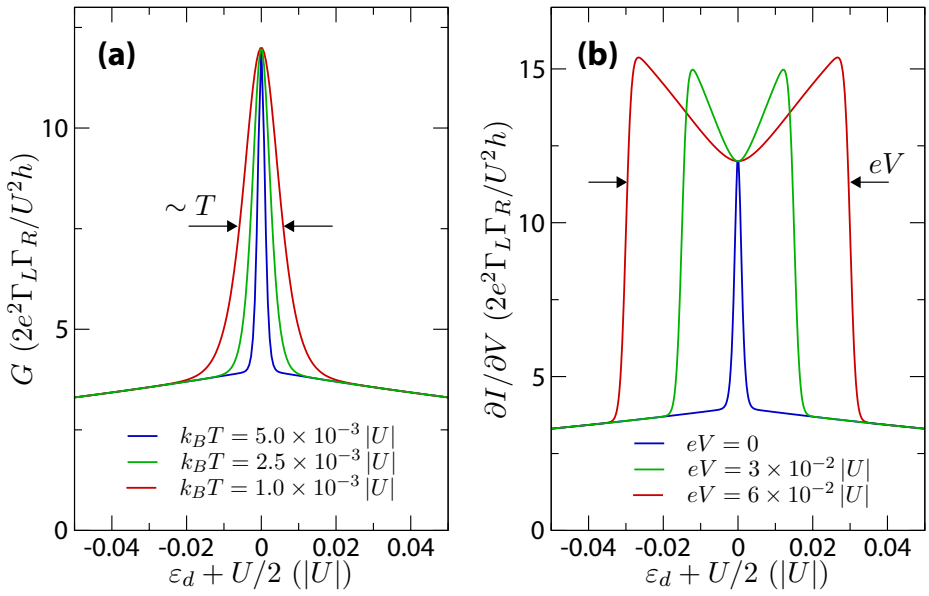

Figure 8.2: Conductance as a function of gate voltage, based on our analytical results. (a) Linear conductance G for several temperatures. The conductance curve exhibits a featureless background due to cotunneling and a distinct peak of constant height and width $\sim T$ due to pair tunneling. (b) Conductance for several bias voltages at $T = 1.0 \times 10^{-3}\,|U|$ for a symmetric junction. For bias voltages $eV \gg k_BT$, the width of the double peak is given by eV.

Here, the last two terms in brackets, which arise from cotunneling, give a slowly varying background. By contrast, pair tunneling, described by the first term in brackets, leads to a remarkable conductance peak. As illustrated in Fig. 8.2(a), its height $G_0 = 24e^2\Gamma_L\Gamma_R/U^2h$ exceeds twice the cotunneling background and is temperature independent, while its width is proportional to T. This feature, which is a direct consequence of the phase space for pair tunneling, should provide an unambiguous experimental signature of pair tunneling as opposed to ordinary Coulomb blockade conductance peaks, whose integral strength is temperature independent.

While the linear conductance is identical for symmetric and asymmetric devices, their finite-bias behavior differs considerably. For large voltages $|eV| \gg k_BT$, we find for the pair tunneling current

$$I^{\text{pairs}} = \frac{e}{\hbar}\frac{16U^2}{(U^2-\delta^2)^2}\frac{2\Gamma_L\Gamma_R}{\Gamma_L^2\,|\delta_+| + \Gamma_R^2\,|\delta_-| + 2\Gamma_L\Gamma_R\,|\delta|} \times \Big[\Theta_+\Gamma_L\,|\delta_+|\,(\Gamma_R\,|\delta_-| + \Gamma_L\,|\delta|) + (L \leftrightarrow R,\, + \leftrightarrow -)\Big], \tag{8.15}$$

where $\delta = 2\varepsilon_d + U$, $\delta_\pm = \delta \pm eV$, and $\Theta_\pm = \theta(-\delta)\theta(\mp\delta_\pm) - \theta(\delta)\theta(\pm\delta_\pm)$. For symmetric devices, Eq. (8.15) implies that the width of the conductance curve is fixed by the bias voltage, as illustrated in Fig. 8.2(b). This behavior is in stark contrast to the conventional Coulomb blockade, where one finds two symmetric sharp peaks at detunings $\pm V/2$ from resonance. This difference which also arises from the phase space for pair tunneling, is further emphasized in Fig. 8.3(a) for all bias and gate voltages.

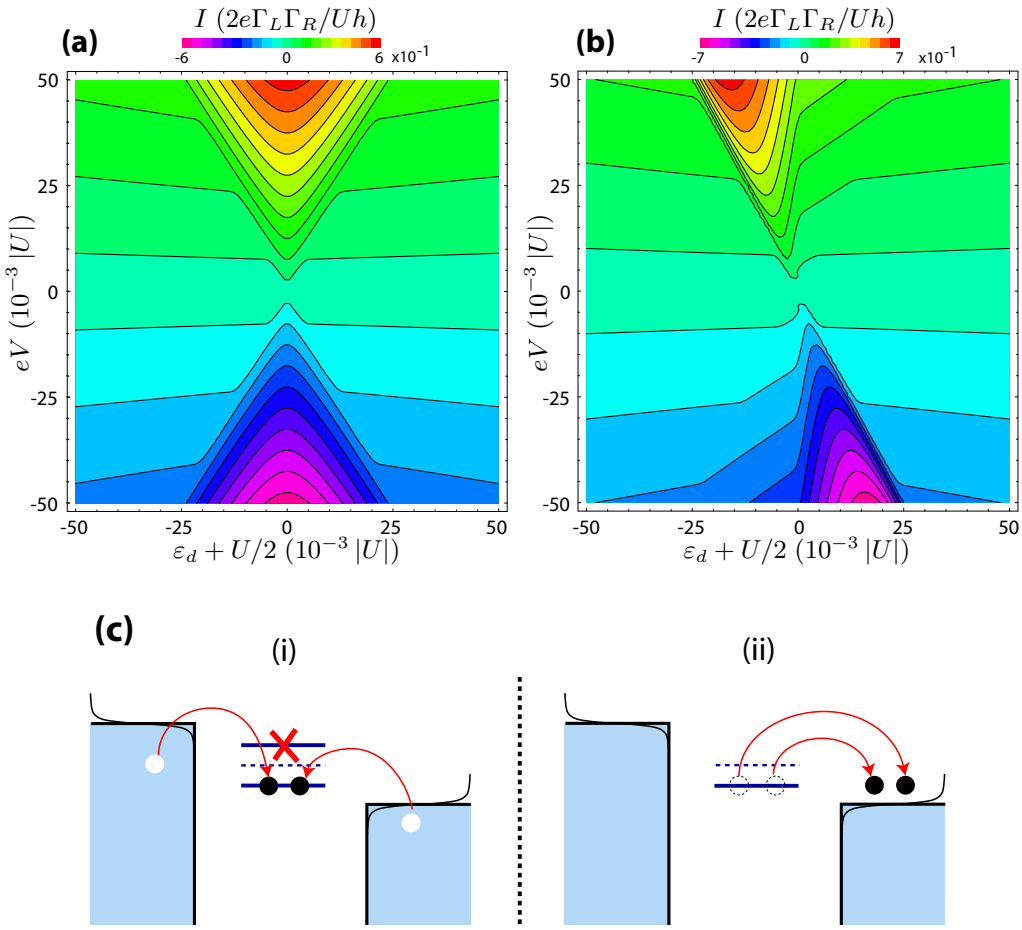

Figure 8.3: Current as a function of bias and gate voltage for (a) a symmetric junction with $\Gamma_L = \Gamma_R = k_BT$, (b) an asymmetric junction with $\Gamma_L = 0.1k_BT$, $\Gamma_R = 10k_BT$, and with $k_BT = 0.5{\cdot}10^{-3}\,|U|$. For asymmetric junctions, one observes the rectification effect due to pair tunneling. (c) Dominant pair-tunneling processes for $\Gamma_R \gg \Gamma_L$ (mixed pair-tunneling process). The gate-voltage dependence of the process (i) explains the possibility of gate-controlled switching in asymmetric devices.

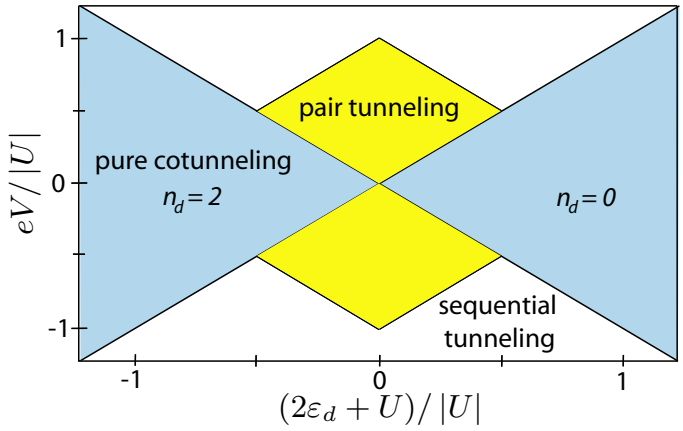

Figure 8.4: Stability diagram for the ground-state occupation n_d and dominant transport modes as a function of gate and bias voltages for a symmetric device with negative U.

Devices with a significant asymmetry in the molecule-lead couplings exhibit a striking asymmetry with respect to voltage inversion, see Fig. 8.3(b). We find in this case that pair tunneling causes strong current rectification, whose transmission direction can be switched by a gate voltage. To understand this rectification effect, consider an asymmetric device with $\Gamma_R \gg \Gamma_L$, and suppose that the Fermi level is higher in the left lead. Then, the pair-tunneling current proceeds by the sequence depicted in Fig. 8.3(c), which call *mixed pair-tunneling process*:

(i) A pair with electrons from opposite leads jumps onto the molecule,

(ii) the electron pair on the molecule is transferred to the right lead.

While (ii) is a fast process ($\sim \Gamma_R^2$), the current is limited by process (i) with rate $\sim \Gamma_L\Gamma_R$. Then, the switching by a gate voltage immediately follows from the rate for process (i), which is exponentially suppressed only for $2\varepsilon_d + U > 0$. By a similar analysis for the opposite bias, one finds an exponential suppression of the pair current for $2\varepsilon_d + U < 0$, thus also explaining the rectification. These features render molecules with negative U interesting candidates for devices with transistor-like characteristics.

8.5 Current shot noise in the negative-U model

As demonstrated in Chapters 3 and 4, a bunching of electrons leads to a characteristic increase of the current noise. Based on this insight, we may expect that transport of electron pairs will also cause interesting fingerprints in the current shot noise. Here, we therefore extend our analysis of pair-tunneling transport and study the zero-frequency noise $S(\omega = 0)$ and the corresponding Fano factor $F = S(\omega = 0)/2e\,|\langle I\rangle|$.

We first present numerical results for the Fano factor, obtained via a generalized version of the technique developed by Korotkov [84]. (Details about the computation can be found in Appendices D and I.2.) Figure 8.5 depicts our results for the Fano factor of a symmetric negative-U device as a function of gate and bias voltage. As expected, the transfer of electrons in pairs is observed to cause super-Poissonian noise $F > 1$ in the regime dominated by pair tunneling. Outside the pair-tunneling regime, cotunneling dynamics leads to purely Poissonian noise, i.e. $F = 1$. The fact that the value $F = 2$, naively expected for electron pairs, is *not* reached, is explained by the coexistence of pair tunneling and cotunneling. We find that the Fano factor maximum for a symmetric device is always concentrated along the crossover boarder between the cotunneling and pair-tunneling regimes. An explanation for this, based on a detailed analysis of pair-tunneling Fano factors, is given below.

As already shown for the current-voltage characteristics, the degree of coupling asymmetry in a negative-U device plays an important role in determining the relevant transport processes. As a result, the noise characteristics crucially depend on the coupling ratio Γ_R/Γ_L, see Figure 8.6. These plots show results for the finite-bias Fano factor as a function of gate voltage, for different coupling ratios. We find that the main effects of a strong coupling asymmetry consist of the suppression of super-Poissonian noise, and the emergence of sub-Poissonian noise in the region dominated by mixed pair-tunneling processes.

Interestingly, it is possible to obtain a comprehensive analytical understanding of the

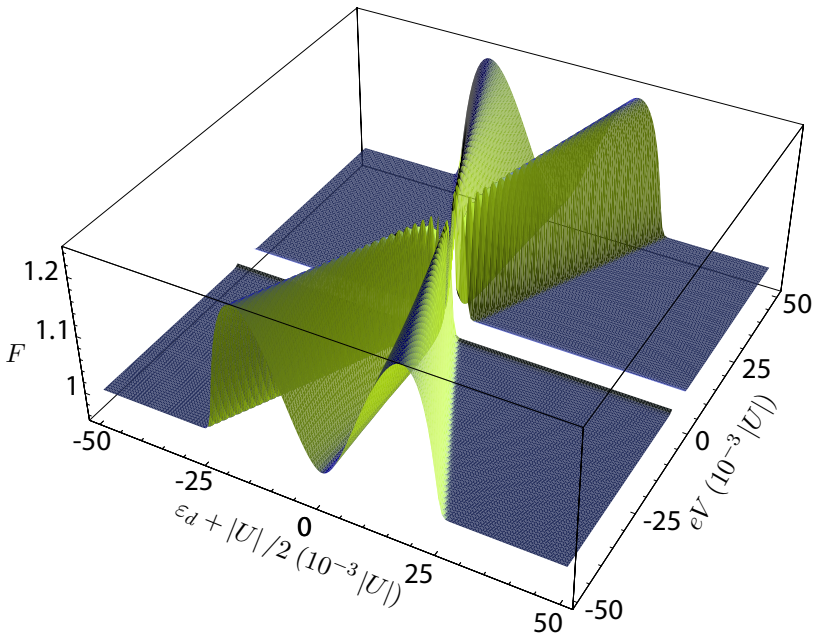

Figure 8.5: Fano factor as a function of bias and gate voltage for a symmetric junction with $\Gamma_L = \Gamma_R = k_BT$, and with $U = -2 \times 10^3 k_BT$. Super-Poissonian noise reflects the bunching of electrons in pair-tunneling processes.

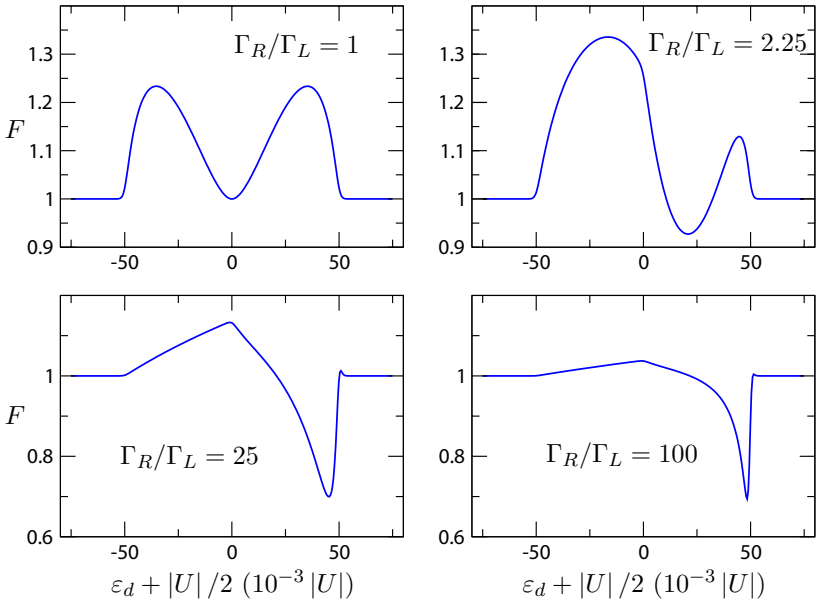

Figure 8.6: Fano factor as a function of gate voltage at finite bias ($eV = 50 \times 10^{-3}|U|$) for different magnitudes of junction asymmetry Γ_L/Γ_R. The dominance of mixed pair-tunneling processes for asymmetric junctions reduces the super-Poissonian noise and leads to Fano factors below 1.

numerical results based on the Fano factor formula derived in Chapter 3,

$$F = \langle N_i \rangle \frac{\langle t_i^2 \rangle - \langle t_i \rangle^2}{\langle t_i \rangle^2} + \frac{\langle N_i^2 \rangle - \langle N_i \rangle^2}{\langle N_i \rangle}. \tag{8.16}$$

In other words, the Fano factor acquires two distinct contributions: The first term in Eq. (8.16) arises from the fluctuations of waiting times t_i, the second term reflects the fluctuations of the number of transferred electrons N_i. Equation (8.16) is valid whenever the quantities N_i and t_i are uncorrelated, and have fixed probability distributions independent of i. Employing this formula, we analytically calculate the separate Fano factors for cotunneling, unidirectional pair tunneling, and mixed pair tunneling in the following.

8.5.1 Fano factor for cotunneling

For temperatures small compared to the applied bias, $k_B T \ll eV$, cotunneling transport is essentially unidirectional: transitions with electron transfer in the direction opposed to the applied bias can be neglected. The current is then determined by a single parameter, the cotunneling rate W. The evaluation of Eq. (8.16) is straightforward. The number of transferred electrons per event is exactly one, and the fluctuations of the transmitted charge vanish. The waiting times t_i follow an exponential distribution $p(t) = We^{-Wt}$, so that the first and second moments are given by

$$\langle t_i \rangle = \frac{1}{W}, \qquad \langle t_i^2 \rangle = \frac{2}{W^2}. \tag{8.17}$$

As a result, cotunneling leads to a Fano factor of unity,

$$F = \frac{\langle t_i^2 \rangle - \langle t_i \rangle^2}{\langle t_i \rangle^2} = 1. \tag{8.18}$$

This explains the Poissonian noise in the regions dominated by cotunneling in Fig. 8.5.

8.5.2 Fano factor for unidirectional pair tunneling

We now consider the case of unidirectional pair tunneling, i.e. transport is assumed to be caused by the following sequence of events: (i) An electron pair tunnels from the left lead onto the molecule. (ii) The electron pair tunnels off of the molecule into the right electrode. When evaluating the Fano factor via Eq. (8.16), we consider events in one of the two junctions. Without loss of generality, we choose the left junction. Then, each event (i) transfers $N_i = 2$ electrons, and there are no fluctuations of this number. However, it is crucial to note that the waiting time t_i now consists of a sum of two times, the waiting time for the event (i) in junction L and the waiting time for event (ii) in junction R, $t_i = t_i^L + t_i^R$. Each waiting time $t_i^{L,R}$ is exponentially distributed according to

$$p_L(t) = W_{0\to 2}^L \exp\left[-W_{0\to 2}^L t\right] \tag{8.19}$$

$$p_R(t) = W_{2\to 0}^R \exp\left[-W_{2\to 0}^R t\right], \tag{8.20}$$

where $W^L_{0\to 2}$ ($W^R_{2\to 0}$) is the rate for the pair-tunneling transition in the left (right) junction. The probability distribution $P(t)$ for the sum of waiting times in the left and right junctions is simply given by the convolution

$$P(t) = \int_0^\infty dt^L \int_0^\infty dt^R\, p_L(t^L) p_R(t^R) \delta(t - t^L - t^R) = \frac{W^L_{0\to 2} W^R_{2\to 0}}{W^R_{2\to 0} - W^L_{0\to 2}} \left[e^{-W^L_{0\to 2} t} - e^{-W^R_{2\to 0} t} \right]. \tag{8.21}$$

The resulting first and second moments of the total waiting time are

$$\langle t_i \rangle = \frac{1}{W^L_{0\to 2}} + \frac{1}{W^R_{2\to 0}} = \frac{W^L_{0\to 2} + W^R_{2\to 0}}{W^L_{0\to 2} W^R_{2\to 0}} \tag{8.22}$$

$$\langle t_i^2 \rangle = 2 \frac{[W^L_{0\to 2}]^2 + W^L_{0\to 2} W^R_{2\to 0} + [W^R_{2\to 0}]^2}{[W^L_{0\to 2}]^2 [W^R_{2\to 0}]^2}. \tag{8.23}$$

Substituting into Eq. (8.16), we obtain for the Fano factor

$$F = \langle N_i \rangle \frac{\langle t_i^2 \rangle - \langle t_i \rangle^2}{\langle t_i \rangle^2} = 2 \frac{(W^R_{2\to 0})^2 + (W^L_{0\to 2})^2}{(W^R_{2\to 0} + W^L_{0\to 2})^2}. \tag{8.24}$$

Due to their phase-space behavior, the pair-tunneling rates vary with gate voltage according to

$$W^L_{0\to 2} \sim \frac{\Gamma_L^2}{h} (eV/2 - \varepsilon_d - U/2) \theta(eV/2 - \varepsilon_d - U/2), \tag{8.25}$$

$$W^R_{2\to 0} \sim \frac{\Gamma_R^2}{h} (\varepsilon_d + U/2 + eV/2) \theta(\varepsilon_d + U/2 + eV/2), \tag{8.26}$$

valid in the limit of low temperatures. Consequently, for a symmetric device the rates are identical at the degeneracy point $2\varepsilon_d + U = 0$, and the Fano factor resulting from Eq. (8.24) is $F = 1$. Away from the degeneracy point, one rate loses phase space while the other gains phase space. As a result, for approximate alignment of the two-particle level with one of the Fermi energies, $\varepsilon_d + U/2 \approx \pm eV/2$, one rate nearly vanishes and the other one remains finite. The corresponding Fano factor is $F = 2$. This dependence of the Fano factor on gate voltage is clearly reflected in the numerical results depicted in Fig. 8.5. Interestingly, for asymmetric devices unidirectional pair-tunneling leads to Fano factors $F > 1$ even at the degeneracy point. In the limit $\Gamma_a/\Gamma_{a'} \to \infty$, one obtains a Fano factor of $F = 2$.

It is worth noting that Eq. (8.24) also yields the Fano factor for sequential tunneling when replacing $\langle N_i \rangle = 2$ by $\langle N_i \rangle = 1$, as well as $W^L_{0\to 2} \to W^L_{0\to 1}$ and $W^R_{2\to 0} \to W^R_{1\to 0}$. The crucial difference between sequential and pair tunneling is that sequential rates are *independent* of gate voltage as long as the level position remains in the bias window. Accordingly, the Fano factor for sequential tunneling in a symmetric device is equal to 1/2.

8.5.3 Fano factor for mixed pair tunneling

Finally, we consider mixed pair tunneling, i.e. the transport mode typical for pair tunneling in asymmetric junctions. Two electrons enter the molecule from the left lead (rate W_1), and subsequently split up to leave the molecule via the left and right junction, respectively

(rate W_2). Let us consider the right junction. Here, exactly one electron is transferred for each combined process of pair tunneling onto and off of the molecule. The waiting time again consists of a sum of two exponentially distributed random times, exactly as in the unidirectional pair-tunneling case. All arguments given there can be reapplied for the case of the mixed pair-tunneling case, resulting in

$$F = \frac{W_1^2 + W_2^2}{(W_1 + W_2)^2}, \tag{8.27}$$

Formally, this is identical to the result for sequential tunneling. Once again, the important difference is the gate-voltage dependence of the pair-tunneling rates. While the phase-space behavior of the rate W_1 is given by Eq. (8.25), the splitting pair rate scales like

$$W_2 \sim \frac{\Gamma_L \Gamma_R}{h}(2\varepsilon_d + U)\theta(2\varepsilon_d + U). \tag{8.28}$$

Consequently, the Fano factor for the mixed pair-tunneling process varies between $F = 1$ and $F = 1/2$, depending on the coupling ratio and gate voltage.

8.5.4 Interpretation of the full Fano factor

The full Fano factor, Fig. 8.5, can now easily be interpreted in terms of the contributions from the previously discussed processes. Outside the pair-tunneling regime, cotunneling is the only relevant process and leads to a Fano factor equal to 1. Inside the pair-tunneling regime, cotunneling, as well as unidirectional and mixed pair tunneling *coexist*. The resulting Fano factor is given by a weighted average of the individual Fano factors.[6] This comprehensively explains the qualitative features of the numerical results in Fig. 8.5, and the fact that the Fano factor does not fully reach the value of 2 naively expected for pair tunneling. As discussed in Section 8.4, for devices with large asymmetry, $\Gamma_a/\Gamma_{a'} \gg 1$, unidirectional pair-tunneling is suppressed and mixed pair processes take over. As a result, the Fano factor is reduced, and sub-Poissonian noise dominates the transport, see Fig. 8.6. The influence of unidirectional pair-tunneling close to the degeneracy point is reflected in remaining super-Poissonian traces for moderate asymmetries.

8.6 Mapping between the negative-U and the conventional Anderson Hamiltonian

We now turn to the mapping between the negative-U and the conventional Anderson model, which we will exploit in subsequent sections in both possible directions for a deeper understanding of each model, both in the high-temperature and Kondo regime. The relation between the positive and negative-U Anderson models was established by Iche and Zawadowski [82], and further elucidated by Haldane [83]. They suggested a particle-hole (PH) transformation for one spin direction, which reverses the sign of the charging energy U and turns the two-particle level position $2\varepsilon_d + U$ in the negative-U picture into a Zeeman field within the positive-U model.

[6] The extraction of the relevant weights is *not* trivial, and Eq. (8.16) cannot be applied in any straightforward way.

This transformation is perfectly suitable for the situation of a negative-U center coupled to one Fermi sea, relevant, e.g., for the case of amorphous semiconductors as discussed by Anderson [128]. However, for the nonequilibrium scenario of transport through a molecule coupled to *two* electrodes, this mapping has the drawback of converting charge current into spin current. For the case of a symmetric device, i.e. symmetric voltage splitting and identical couplings to the left and right electrode, we show that a subsequent left-right (LR) transformation eliminates this problem. In combination, the resulting particle-hole/left-right (PHLR) transformation provides an exact mapping between the charge currents in the negative-U model and the conventional Anderson model with local Zeeman field.

The key effect of the PHLR transformation is given by the mapping of charge to spin degrees of freedom. It is precisely this interchangeability which establishes the relation between the spin degeneracy leading to the conventional spin-Kondo effect and the charge degeneracy causing the charge-Kondo effect. Importantly, the PHLR transformation also implies that particle-hole symmetry within one model is mapped to spin symmetry within the counterpart model (and vice versa). As a consequence, the breaking of particle-hole symmetry by tuning the gate-voltage in the negative-U model exactly corresponds to the breaking of spin symmetry by a local Zeeman field in the positive-U model. Thus, recalling that spin-symmetry breaking inhibits the conventional Kondo effect, the PHLR mapping immediately explains the fragility of the charge-Kondo effect as a function of gate voltage.

We first review the PH mapping, following References [82] and [83], and subsequently introduce the LR mapping.

8.6.1 Particle-hole transformation

The PH transformation is carried out for one of the two spin directions, and without loss of generality we may choose $\sigma = \downarrow$. We define new annihilation and creation operators β, $\beta^\dagger$ by

$$\beta_{d\uparrow} \equiv d_\uparrow, \qquad \beta_{a\mathbf{p}\uparrow} \equiv c_{a\mathbf{p}\uparrow}, \tag{8.29}$$

$$\beta_{d\downarrow} \equiv d^\dagger_\downarrow, \qquad \beta_{a\mathbf{p}\downarrow} \equiv -c^\dagger_{a(-\mathbf{p})\downarrow}. \tag{8.30}$$

In other words, for $\sigma = \uparrow$ we continue speaking of creation and annihilation of particles, whereas for $\sigma = \downarrow$ we describe the system in terms of creation and annihilation of holes. It is straightforward to verify that the β operators obey the usual anticommutation rules. We define the corresponding number operators by $\bar{n}_{d\sigma} \equiv \beta^\dagger_{d\sigma}\beta_{d\sigma}$ and $\bar{n}_{a\mathbf{p}\sigma} \equiv \beta^\dagger_{a\mathbf{p}\sigma}\beta_{a\mathbf{p}\sigma}$. From this, one immediately infers that

$$n_{d\uparrow} = \bar{n}_{d\uparrow}, \qquad n_{a\mathbf{p}\uparrow} = \bar{n}_{a\mathbf{p}\uparrow}, \tag{8.31}$$

$$n_{d\downarrow} = 1 - \bar{n}_{d\downarrow}, \qquad n_{a\mathbf{p}\downarrow} = 1 - \bar{n}_{a(-\mathbf{p})\downarrow}. \tag{8.32}$$

With this PH transformation, the negative-U Hamiltonian (up to an irrelevant additive constant) is mapped to

$$\begin{aligned}\bar{H} =& \frac{U}{2}\sum_\sigma \bar{n}_{d\sigma} - U\bar{n}_{d\uparrow}\bar{n}_{d\downarrow} + \sum_{a\mathbf{p}\sigma}\epsilon_{a\mathbf{p}}\bar{n}_{a\mathbf{p}\sigma} \\ &- \sum_{a\mathbf{p}\sigma} a\sigma\frac{eV}{2}\bar{n}_{a\mathbf{p}\sigma} + \sum_{a\mathbf{p}\sigma}\left(t_{a\mathbf{p}}\beta^\dagger_{a\mathbf{p}\sigma}\beta_{d\sigma} + t^*_{a\mathbf{p}}\beta^\dagger_{d\sigma}\beta_{a\mathbf{p}\sigma}\right) + (\varepsilon_d + U/2)(\bar{n}_{d\uparrow} - \bar{n}_{d\downarrow}).\end{aligned} \tag{8.33}$$

Here, we have used the identity $t_{a(-\mathbf{p})} = t^*_{a\mathbf{p}}$ in order to rearrange the expression for the tunneling Hamiltonian, and we have assumed a particle-hole symmetric band, i.e. $\epsilon_{a(-\mathbf{p})} = -\epsilon_{a\mathbf{p}}$. [Note that this is generically true in the vicinity of the Fermi energy by linearizing the dispersion relation.] Analyzing the resulting expression for the Hamiltonian, one notes that the Anderson model with negative U has been mapped to an Anderson model with positive $U' = -U$ and an additional Zeeman energy B'. Denoting all parameters of the new Hamiltonian with primes, we can set up the following "dictionary":

$$\varepsilon'_d = U/2, \quad U' = -U, \quad B' = 2\varepsilon_d + U. \tag{8.34}$$

Note that the current through the system, originally given by

$$\langle I \rangle = \frac{e}{2} \left\langle \frac{d}{dt} \sum_{a\mathbf{p}\sigma} a\, n_{a\mathbf{p}\sigma} \right\rangle, \tag{8.35}$$

now takes the form

$$\langle I \rangle = \frac{e}{2} \left\langle \frac{d}{dt} \sum_{a\mathbf{p}\sigma} a\sigma \bar{n}_{a\mathbf{p}\sigma} \right\rangle. \tag{8.36}$$

As evident from the additional spin factor in the current, the PH transformation turns the charge current of the negative-U model into a spin current in the conventional Anderson model (and vice versa).

8.6.2 Left-right transformation

In order to obtain a transformation which maps charge current to charge current, we exploit the assumption of a symmetric device and perform the following left-right transformation,

$$d'_\sigma \equiv \beta_{d\sigma}, \qquad c'_{a\mathbf{p}\uparrow} \equiv \beta_{a\mathbf{p}\uparrow}, \tag{8.37}$$

$$c'_{L\mathbf{p}\downarrow} \equiv \beta_{R\mathbf{p}\downarrow}, \qquad c'_{R\mathbf{p}\downarrow} \equiv \beta_{L\mathbf{p}\downarrow}. \tag{8.38}$$

While the $\sigma =\uparrow$ component remains invariant, the $\sigma =\downarrow$ electrons (specifically, the spin component which was previously affected by the particle-hole transformation) acquire an interchange of the labels for left and right. This transforms the Hamiltonian $\bar{H}$ into

$$\begin{aligned} H' = {} & \frac{U}{2} \sum_\sigma n'_{d\sigma} - U n'_{d\uparrow} n'_{d\downarrow} + \sum_{a\mathbf{p}\sigma} (\epsilon_{a\mathbf{p}} - aeV/2) n'_{a\mathbf{p}\sigma} \\ & + \sum_{a\mathbf{p}\sigma} \left(t_{\mathbf{p}} c'^\dagger_{a\mathbf{p}\sigma} d'_\sigma + t^*_{\mathbf{p}} d'^\dagger_\sigma c'_{a\mathbf{p}\sigma} \right) + (\varepsilon_d + U/2)(n'_{d\uparrow} - n'_{d\downarrow}). \end{aligned} \tag{8.39}$$

Here, the crucial point is that the bias now affects both spin components in the same way, and the current is expressed as

$$\langle I \rangle = \frac{e}{2} \left\langle \frac{d}{dt} \sum_{a\mathbf{p}\sigma} a n'_{a\mathbf{p}\sigma} \right\rangle. \tag{8.40}$$

Through the combined PHLR mapping, the charge current of the negative-U model is thus mapped to a charge current of the positive-U Anderson model.

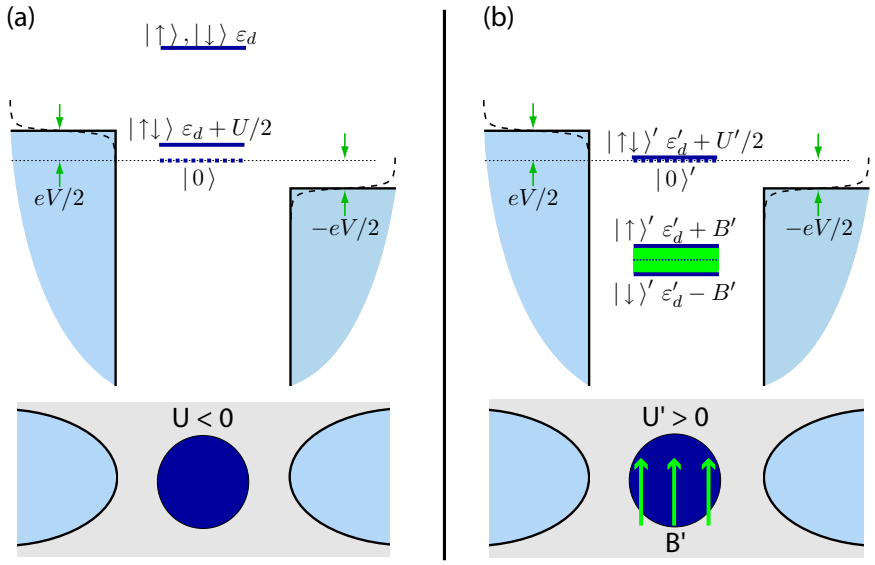

Figure 8.7: Illustration of the mapping between the negative-U model (a) and the conventional Anderson model (b) with additional local Zeeman field B'. All level energies are given as energies per particle.

As a result, we have established a one-to-one mapping between transport in the negative-U model and transport in a conventional Anderson model with an additional local Zeeman field acting on the molecule. The magnitude of the Zeeman field is determined by the detuning of the two-particle level from the degeneracy point with the unoccupied molecule. In the negative-U model, this detuning is essentially given by the gate voltage. Further, observing that the new one-particle energy and charging energy are given by $\varepsilon'_d = U/2$ and $U' = -U$, respectively, we emphasize that the conventional Anderson model is fixed to the symmetric point $2\varepsilon'_d + U' = 0$. This is a direct consequence of the fact that the PHLR transformation maps the negative-U spin symmetry to particle-hole symmetry in the positive-U model. An illustration of the resulting configuration is provided in Fig. 8.7. The details of the mapping are summarized by the "dictionary" in Table 8.1.

8.6.3 Mapping for the linear-response regime

It is important to note that the PHLR mapping crucially depends on the assumption of a device with symmetric voltage splitting and identical couplings to the left and right lead. In view of realistic experimental setups, this amounts to a rather strict assumption. In this subsection, we show that for the linear-response regime ($V \to 0$), the mapping between negative- and positive-U models remains valid even for asymmetric couplings, $\Gamma_L \neq \Gamma_R$. The discussion of the more general finite-bias case with asymmetric couplings is deferred to Section 8.10.

Let us define V_σ and I_σ as the spin-dependent bias and current in the negative-U Anderson model, and V'_σ and I'_σ as the corresponding quantities in the positive-U model. Then, restricting to the linear-response regime, the current in the negative-U model has the

negative-U model	**Anderson model**
mol. operators:	mol. operators:
$d_\uparrow$, $d_\downarrow$	$d'_\uparrow$, $d'^\dagger_\downarrow$
lead operators:	lead operators:
$c_{a\mathbf{p}\uparrow}$, $c_{L\mathbf{p}\downarrow}$, $c_{R\mathbf{p}\downarrow}$	$c'_{a\mathbf{p}\uparrow}$, $-c'^\dagger_{R(-\mathbf{p})\downarrow}$, $-c'^\dagger_{L(-\mathbf{p})\downarrow}$
mol. states:	mol. states:
$\lvert 0\rangle$, $\lvert\uparrow\rangle$, $\lvert\downarrow\rangle$, $\lvert\uparrow\downarrow\rangle$	$\lvert\downarrow\rangle'$, $\lvert\uparrow\downarrow\rangle'$, $\lvert 0\rangle'$, $\lvert\uparrow\rangle'$
	charging energy
charging energy	$U' = -U > 0$
$U < 0$	gate voltage
	$\varepsilon'_d = U/2$
gate voltage	Zeeman energy
ε_d	$B' = 2\varepsilon_d + U$

Table 8.1: Dictionary for the mapping between the negative-U model and the conventional Anderson model with additional Zeeman field. Symbols with (without) primes denote quantities in the positive-U (negative-U) model.

form

$$I_\uparrow = g_{\uparrow\uparrow}V_\uparrow + g_{\uparrow\downarrow}V_\downarrow \qquad I_\downarrow = g_{\downarrow\uparrow}V_\uparrow + g_{\downarrow\downarrow}V_\downarrow, \tag{8.41}$$

where $g_{\sigma\sigma'}$ denotes the conductance response of spin-σ electrons to a bias voltage applied to spin-σ' electrons only. Accordingly, the total linear conductance of the negative-U Anderson model is obtained by dividing $I_\uparrow + I_\downarrow$ by $V = V_\uparrow = V_\downarrow$, resulting in

$$G = \sum_{\sigma\sigma'} g_{\sigma\sigma'}. \tag{8.42}$$

On the other hand, we may evaluate the linear conductance of the positive-U model by exploiting the PH transformation. As a result of Eq. (8.36), the charge current $I = I_\uparrow + I_\downarrow$ of the negative-U model is turned into a spin current in the positive-U model. Simultaneously, the bias sign for spin-$\downarrow$ electrons is inverted, so that we have

$$I'_\uparrow = I_\uparrow = g_{\uparrow\uparrow}V'_\uparrow - g_{\uparrow\downarrow}V'_\downarrow, \tag{8.43}$$

$$I'_\downarrow = -I_\downarrow = -g_{\downarrow\uparrow}V'_\uparrow + g_{\downarrow\downarrow}V'_\downarrow. \tag{8.44}$$

Setting $V'_\uparrow = V'_\downarrow = V'$ we obtain the linear conductance of the positive-U model

$$G' = g_{\uparrow\uparrow} + g_{\downarrow\downarrow} - g_{\uparrow\downarrow} - g_{\downarrow\uparrow}. \tag{8.45}$$

Now we prove that $g_{\uparrow\downarrow} = g_{\downarrow\uparrow} = 0$, which gives the desired result, $G = G'$. To see that, one can use the Glazman-Raikh transformation [129] (see Appendix A.3), and write the current operator in the form

$$I = -\frac{i}{\hbar}\frac{|t_L|\,|t_R|}{\sqrt{|t_L|^2 + |t_R|^2}} \sum_{\mathbf{p}\sigma} \left[\psi^\dagger_{2\mathbf{p}\sigma} d_\sigma - \text{h.c.}\right], \tag{8.46}$$

where ψ_2 denotes the *decoupled* lead. Due to this decoupling of ψ_2, it is impossible to fully contract the current-current correlator $\langle I_\uparrow I_\downarrow\rangle$ and the off-diagonal response functions giving the conductivities $g_{\sigma\bar{\sigma}}$ vanish.

8.7 Positive-U model with local Zeeman field: High-temperature regime

Although the central goal of this chapter consists of an analysis of transport in the negative-U model, we first exploit the PHLR transformation in the opposite direction and investigate the positive-U model with local Zeeman field. Intriguingly, the mapping opens up a new way of understanding the effects of a local Zeeman field on transport in the Anderson model at high temperatures, $T \gg T_K$. Based on our previous findings for the negative-U model, which revealed super-Poissonian Fano factors $F > 1$ due to tunneling of electron pairs, the mapping surprisingly dictates that an identical enhancement of Fano factors must also occur due to the presence of the Zeeman field at positive U. After analyzing the linear conductance and nonlinear current-voltage characteristics, we will pinpoint the cotunneling correlations due to the Zeeman field as the origin for super-Poissonian noise by translating the pair-tunneling processes into the positive-U language.

8.7.1 Linear conductance and current-voltage characteristics

For temperatures large compared to the Kondo temperature, we have shown in the previous sections that transport in the negative-U case is dominated by sequential tunneling of *electron pairs*. By means of the PHLR transformation, we can now translate our analytical results obtained for the negative-U model to the positive-U Anderson model. Its linear conductance is dominated by cotunneling, and as a function of the local Zeeman field B' it is given by

$$G' = \frac{2e^2\Gamma_L\Gamma_R}{h}\left[\frac{U'^2}{(U'+B')^2(U'-B')^2}\frac{8\beta B'}{\sinh[\beta B']} + f(-B')\frac{4}{(U'+B')^2} + f(B')\frac{4}{(U'-B')^2}\right]. \tag{8.47}$$

Here, the first term is caused by inelastic spin-flip processes, the last two terms are generated by elastic cotunneling. The mapping between the processes at positive U and the corresponding pair-tunneling and cotunneling processes in the negative-U model are illustrated in Figures 8.8 and 8.9. In analogy to the increased phase space for two-particle processes at negative U, inelastic spin-flip processes gain a phase-space enhancement proportional to $|\pm eV/2 - B'|$ whenever $|B'| < eV/2$. As a result, the linear conductance G' develops a peak for vanishing Zeeman field. The peak width is given by temperature and its height is constant. This is the exact counterpart of the pair-tunneling conductance peak at negative U.

Similarly, the nonlinear current-voltage characteristics $I(\varepsilon_d, V)$ for the negative-U model can be mapped to the current of the positive-U Anderson model as a function of Zeeman field and bias voltage, $I'(B', V)$. In particular, in the limit of small temperatures we obtain for the current due to inelastic cotunneling (spin-flips)

$$\begin{aligned} I^{\text{inel}} =& \frac{e}{\hbar}\frac{16U'^2}{(U'^2-\delta^2)^2}\frac{2\Gamma_L\Gamma_R}{\Gamma_L^2|\delta_+| + \Gamma_R^2|\delta_-| + 2\Gamma_L\Gamma_R|\delta|} \\ &\times\left[\Theta_+\Gamma_L|\delta_+|\left(\Gamma_R|\delta_-| + \Gamma_L|\delta|\right) + (L\leftrightarrow R, +\leftrightarrow -)\right], \end{aligned} \tag{8.48}$$

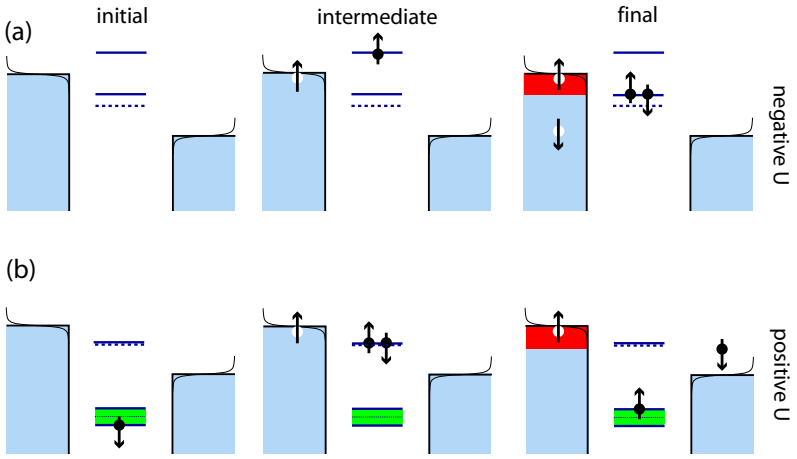

Figure 8.8: Relation between (a) the unidirectional pair-tunneling process for negative U and (b) the inelastic spin-flip in the conventional Anderson model with local Zeeman field, as obtained by the PHLR transformation. The phase space available for each process is marked in red color.

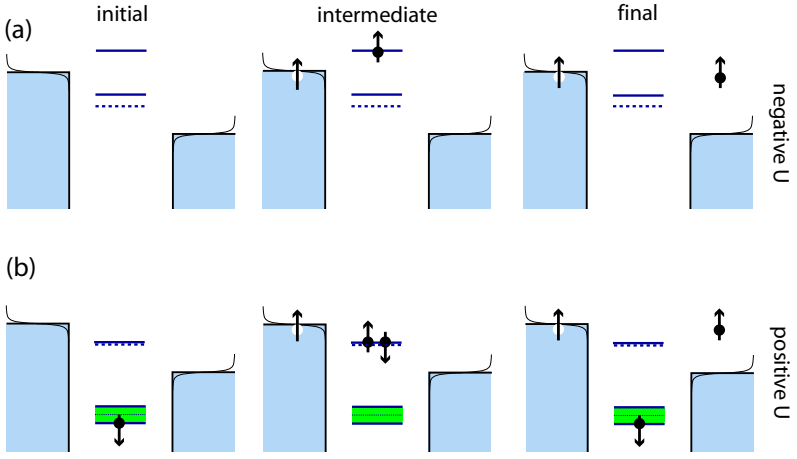

Figure 8.9: Relation between (a) the elastic cotunneling process for negative U and (b) elastic cotunneling in the conventional Anderson model with local Zeeman field, as obtained by the PHLR transformation.

where $\delta = B'$, $\delta_\pm = \delta \pm eV$, and $\Theta_\pm = \theta(-\delta)\theta(\mp\delta_\pm) - \theta(\delta)\theta(\pm\delta_\pm)$. Analogous to the pair-tunneling current, this spin-flip current dominates the transport properties whenever the Zeeman field is smaller than the bias window, $|eV|/2 \geq |B'|$.

8.7.2 Current shot noise in the positive-U Anderson model

The PHLR mapping can now easily be employed to extract the corresponding results for the Fano factor in the positive-U Anderson model. As a result of the mapping, the gate-voltage axis in Fig. 8.5 is converted to the Zeeman field $B'/2$. Evidently, the presence of the local Zeeman field leads to super-Poissonian noise. The origin of this noise enhancement can be traced back to the translation of the unidirectional pair tunneling into the language of the positive-U Anderson model. Applying the PHLR transformation, one finds that the two consecutive pair processes correspond to two inelastic cotunneling processes, see Fig. 8.8: The first process flips the spin from down to up, the second process flips it back to $\sigma = \downarrow$. In both cases, one electron is transferred from the left to the right lead. The crucial point is that these two processes are correlated whenever the Zeeman field is nonzero. For $B' \neq 0$, the phase-space involved in the inelastic processes causes one spin-flip to be faster than the other one. The difference of the rates becomes maximal when the Zeeman field becomes as large as the bias voltage, $B' \approx eV$.

8.8 The onset of the Kondo effect: Logarithmic corrections

Now, we return to the focus of this chapter on negative charging energies, and employ the PHLR transformation to deepen our understanding of the negative-U model based on the conventional Anderson model. It is known that the degeneracy between the two charge states $n = 0$ and $n = 2$ in the negative-U Anderson model results in Kondo correlations at low temperatures [122]. For temperatures $T \gg T_K$, the development of these correlations is expected to be signalled by logarithmic corrections to the leading-order perturbative results. Here, we exploit the PHLR transformation to extract the logarithms for the negative-U case from well-known results in the context of the conventional Anderson model, see e.g. Ref. [14].

Specifically, the chain of transformations we employ is as follows. Our starting point is the negative-U Anderson model. Applying the PHLR transformation, we obtain a conventional Anderson model with local Zeeman field, Eq. (8.39). Then, a Schrieffer-Wolff transformation [126] is performed. Up to an irrelevant renormalization of the level energy ε_d, the mapping results in $H' = H_0 + H_\mathrm{J} + H_\mathrm{pot} + H_\mathrm{Z}$, where

$$H_0 = \varepsilon_d + \sum_{a\mathbf{p}\sigma} \epsilon_{a\mathbf{p}} c^\dagger_{a\mathbf{p}\sigma} c_{a\mathbf{p}\sigma}, \tag{8.49}$$

$$H_\mathrm{J} = \sum_{aa'\mathbf{pp}'} J_{aa'\mathbf{pp}'} \mathbf{s}_{aa'\mathbf{pp}'} \cdot \mathbf{S}, \tag{8.50}$$

$$H_\mathrm{pot} = \sum_{aa'\mathbf{pp}'\sigma} K_{aa'\mathbf{pp}'} c^\dagger_{a\mathbf{p}\sigma} c_{a'\mathbf{p}'\sigma}, \tag{8.51}$$

$$H_\mathrm{Z} = B' S^z \tag{8.52}$$

Further details about the Schrieffer-Wolff transformation including definitions of the amplitudes J and K are deferred to Appendix A.2. In order to make the connection to the Kondo-Hamiltonian [13], the dependence of the amplitudes J and K on energy is approximated by their Fermi-energy values within a band of width D and zero outside. That is, inside the band we have

$$J_{aa'} = -2t_a t^*_{a'} \frac{U'}{(\varepsilon'_d + U')\varepsilon'_d} = -8t_a t^*_{a'} \frac{1}{U} \tag{8.53}$$

$$K_{aa'} = -\frac{t_a t^*_{a'}}{2} \frac{2\varepsilon'_d + U'}{\varepsilon'_d(\varepsilon'_d + U')} = 0. \tag{8.54}$$

Since the PHLR transformation maps the negative-U model onto an Anderson model fixed to the symmetry point $2\varepsilon'_d + U' = 0$, the potential scattering term is identically zero, and the resulting Hamiltonian is

$$H_K = H_0 + \sum_{aa'} J_{aa'} \mathbf{s}_{aa'} \cdot \mathbf{S} + B' S^z. \tag{8.55}$$

In the linear response regime (zero bias), the Hamiltonian may be further simplified by exploiting that the Hermitian matrix $\mathsf{J} = (J_{aa'})$ has the eigenvalues 0 and $J = -(8/U)\sum_a |t_a|^2$. This exchange coupling $J > 0$ is antiferromagnetic, leading to a screening of the local spin by the conduction electrons and the formation of a spin-singlet state for $T \ll T_K$, discussed in the subsequent section. In terms of the eigenvectors of J, the original two-leads problem can therefore be written as a one-channel problem [14],

$$H'_K = \sum_i \sum_{\mathbf{p}\sigma} \epsilon_{\mathbf{p}} \psi^\dagger_{i\mathbf{p}\sigma} \psi_{i\mathbf{p}\sigma} + J \mathbf{s}_1 \cdot \mathbf{S} + B' S^z. \tag{8.56}$$

Alternatively, this can be derived by applying the Glazman-Raikh transformation [129] to the Anderson Hamiltonian before carrying out the Schrieffer-Wolff transformation.

After mapping the negative-U problem to the Kondo Hamiltonian, it is straightforward to translate results from the conventional spin-Kondo effect to the charge-Kondo scenario of negative U. In particular, a perturbative treatment of the exchange coupling leads to the well-known logarithmic terms $\sim J^2 \ln(D/\omega)$ in the amplitude for a transition $|\,\mathbf{p}s, \sigma\,\rangle \to |\,\mathbf{p}'s', \sigma'\,\rangle$ [13, 14]. Summing up the most-diverging contributions to all orders, or using poor-man's scaling alternatively [130], results in the emergence of the Kondo temperature

$$T_K = D \exp[-1/\rho J], \tag{8.57}$$

where ρ denotes the density of states of the leads. Employing the Kubo formula, the conductance for vanishing Zeeman field $B' = 2\varepsilon_d + U = 0$ is found to be

$$G = \frac{2e^2}{h} \frac{4\Gamma_L \Gamma_R}{(\Gamma_L + \Gamma_R)^2} \frac{3\pi^2}{16} \frac{1}{\ln^2(T/T_K)}. \tag{8.58}$$

Note that the leading order correctly reproduces the rate-equations result for the pair-tunneling peak: For $T \gg T_K$ we have $\ln(T/T_K) \approx \rho J$, so that

$$G \approx 24 e^2 \Gamma_L \Gamma_R / U^2 h. \tag{8.59}$$

For decreasing temperature, the developing Kondo correlations cause a slow logarithmic increase of the peak height value. Additional corrections affect the tails of the conductance peak. In the language of the positive-U Anderson model, this implies considering the situation of a large Zeeman field $B' = 2\varepsilon_d + U \gg k_B T$. For this limit, a relation similar to Eq. (8.58) can be derived [14], namely

$$G = \frac{2e^2}{h} \frac{4\Gamma_L \Gamma_R}{(\Gamma_L + \Gamma_R)^2} \frac{\pi^2}{16} \frac{1}{\ln^2[(2\varepsilon_d + U)/T_K]}. \tag{8.60}$$

This captures the logarithmic corrections to the cotunneling tails of the conductance peak in the negative-U model.

8.9 The charge-Kondo regime

The logarithmic corrections considered in the previous section signal the onset of the charge-Kondo effect in the negative-U model. In this section, we turn to the investigation of the Kondo effect in the low-temperature regime, $T \ll T_K$. Again, the PHLR transformation serves as a central tool in our considerations, allowing for the translation of the conventional spin-Kondo effect into the charge-Kondo effect.

We start with a brief review of the conventional spin-Kondo regime. In the previous section, we have seen that, for temperatures $T \gg T_K$, the effective exchange coupling J grows with decreasing temperature, diverging at the Kondo temperature due to the breakdown of perturbation theory. The true low-temperature behavior of the system was first discussed independently by Anderson [131], Yosida [132], and Yoshimori [133]. They concluded that the Kondo regime is described by the strong-coupling limit $J \gg D$, which causes the trapping of one conduction electron at the impurity site and the formation of a spin-singlet state.

Despite the intricate many-body nature of the Kondo effect, the low-temperature limit $T \to 0$ again becomes remarkably simple. As demonstrated by Nozières [134, 135], the locking into a spin-singlet state leaves only a *nonmagnetic* impurity and the remaining conduction electrons. At finite temperatures $0 < k_B T \ll J$, real breaking of the singlet state is energetically impossible, but virtual excursions into the $n = 0, 2$ and $n = 1$-triplet states occur. This polarizability of the singlet generates a weak effective electron-electron interaction. Following Nozières, the low-temperature limit is accurately described by a Landau Fermi-liquid theory, and is captured by the effective Hamiltonian

$$\begin{aligned} H = &\sum_{k\sigma} \xi_k \psi^\dagger_{k\sigma} \psi_{k\sigma} - \frac{1}{\pi \rho T_K} \sum_{k,k'\sigma} \big(\alpha \frac{\xi_k + \xi_{k'}}{2} + \gamma B' \sigma\big) \psi^\dagger_{k\sigma} \psi_{k'\sigma} \\ &+ \frac{\beta}{\pi \rho^2 T_K} \sum_{k_1,k_2,k_3,k_4} \psi^\dagger_{k_1\uparrow} \psi_{k_2\uparrow} \psi^\dagger_{k_3\downarrow} \psi_{k_4\downarrow}, \end{aligned} \tag{8.61}$$

where $\psi_{k\sigma}$ annihilates a quasiparticle with energy $\xi_k = v_F k$ and spin σ.[7] The α-term describes the quasiparticle scattering at the impurity site, the β-term accounts for the induced interaction between quasiparticles. As shown by Nozières, a central consequence of

[7] Note that we set $k_B = 1$ in the present section.

the fact that the Kondo resonance is always floating on the Fermi sea, consists of the fixing of the parameter ratio α/β to unity [134, 135]. The additional γ-term describes the effect of a local Zeeman field B' acting on the impurity (as generated by the PHLR mapping). We note that both coefficients α and γ may be determined by a comparison with the exact Bethe-ansatz solution [136], leading to $\alpha = \gamma = T_K/T_K^{ba}$ with $T_K^{ba} = \frac{(2U\Gamma)^{1/2}}{\pi} e^{-\frac{\pi U}{8\Gamma}}$.

8.9.1 Linear conductance

In Section 8.6.3, we have established the equality of the conductances for the positive-U and negative-U models. Here, we exploit this finding to obtain the low-temperature conductance of the negative-U model in the Kondo regime, based on our knowledge of the conventional spin-Kondo effect at positive U.

Within the Fermi-liquid description, the linear conductance may be expressed as a function of the scattering phase shift. As shown by Nozières in Ref. [134], this phase shift depends both on the energy of the incoming particle and on the particle distribution, and can be expanded as

$$\delta_\sigma = \frac{\pi}{2} + \frac{\alpha\epsilon}{T_K} - \frac{\beta n_{\bar\sigma}}{\rho T_K} + \frac{\gamma\sigma B'}{T_K}. \tag{8.62}$$

Here, spin inversion is denoted by $\bar\sigma = -\sigma$, and ρ is the density of states. The leading-order phase shift $\pi/2$ makes the molecule a perfectly open channel in the Kondo regime. From the phase shift we can determine the transmission and reflection amplitudes from left to right (from right to left), t_σ and r_σ (t'_σ and r'_σ), respectively. t_σ. Using the Glazman-Raikh transformation [129], we easily obtain the corresponding scattering matrix

$$\mathsf{S}_\sigma(\epsilon) = \begin{pmatrix} r_\sigma & t'_\sigma \\ t_\sigma & r'_\sigma \end{pmatrix} = \begin{pmatrix} c & -s \\ s & c \end{pmatrix} \begin{pmatrix} e^{2i\delta_\sigma} & 0 \\ 0 & 1 \end{pmatrix} \begin{pmatrix} c & s \\ -s & c \end{pmatrix}, \tag{8.63}$$

where $(c, s) = \frac{(|t_L|, |t_R|)}{\sqrt{\sum_a |t_a|^2}}$. This results in a transmission coefficient given by

$$|t_\sigma|^2 = \frac{4\,|t_L|^2\,|t_R|^2}{(|t_L|^2 + |t_R|^2)^2} \sin^2(\delta_\sigma). \tag{8.64}$$

At $T = 0$, the linear conductance is not expected to depend on α nor β since the corresponding processes involve quasiparticles with finite energies. As a result, the Kondo-regime conductance of the Anderson model with local Zeeman field $B' \ll T_K$ is given by

$$G' = \frac{e^2}{h} \sum_\sigma |t_\sigma^2| = \frac{2e^2}{h} \frac{4\Gamma_L\Gamma_R}{(\Gamma_L + \Gamma_R)^2} \left[1 - (\gamma B'/T_K)^2\right]. \tag{8.65}$$

Employing the identity of linear conductances for the positive and negative-U models, see Section 8.6.3, we conclude that the charge-Kondo effect in the negative-U model leads to the conductance

$$G = \frac{2e^2}{h} \frac{4\Gamma_L\Gamma_R}{(\Gamma_L + \Gamma_R)^2} \left[1 - \left(\frac{\gamma}{T_K}[2\varepsilon_d + U]\right)^2\right]. \tag{8.66}$$

Here, the correspondence between Zeeman field (at positive U) and gate voltage (at negative U) is directly reflected in the departure from the unitary limit as soon as the negative-U system is tuned away from the charge-degeneracy point. This marks the fragility of the charge-Kondo effect in contrast to the conventional Kondo effect.

8.9.2 Nonlinear current-voltage characteristics

We now go beyond the linear-response regime and consider the nonlinear conductance of the symmetric positive and negative-U models in the $T = 0$ limit. Our starting point is the positive-U model, which results in the conventional Kondo effect. The PHLR tranformation is applied subsequently to transfer our results to the charge-Kondo case at negative U.

For nonzero bias, quasiparticles with finite energy are involved, and hence the α- and β-terms in the effective Hamiltonian, Eq. (8.61), become relevant. These terms describe the weak scattering at the spin-singlet state and the induced interaction between quasiparticles, and cause a reduction of the unitary current $I_u = 2e^2/h\,V$ due to backscattering events. The total current may thus be written in the form $I = I_u - I_b$. In order to extract the backscattering contributions from the effective Hamiltonian, we need to relate the quasiparticle states $\psi_{k\sigma}$ to the states of left-movers and right-movers, $L_{k\sigma}$ and $R_{k\sigma}$, respectively. This relation is dictated by the Glazman-Raikh transformation [129], which results in

$$\psi_{k\sigma} = \frac{1}{\sqrt{2}}(L_{k\sigma} + R_{k\sigma}) \tag{8.67}$$

for a symmetric device.[8] Importantly, left-movers originate from the right lead and right-movers from the left lead. This fact allows us to account for the nonequilibrium situation at finite bias by identifying the distribution of right-movers (left-movers) with the Fermi distribution of the left (right) lead, i.e. $f_{L(R)}(\epsilon)$. Substituting the decomposition Eq. (8.67) into the effective Hamiltonian, we find that the elastic term ($\sim \alpha$) and the inelastic term ($\sim \beta$) generate backscattering transitions which turn left-movers into right-movers, and vice versa. Since these contributions act as weak perturbations, we may evaluate the backscattering current by summing the corresponding backscattering rates obtained via Fermi's golden rule. Our approach reproduces the well-established results from Ref. [14], and here we briefly review the essential steps, starting with the elastic contributions.

Elastic backscattering contributions

Upon substitution of the left-right decomposition, the elastic contribution to the effective Hamiltonian can be cast into the form

$$H_{\rm el} = -\frac{1}{2\pi\rho T_K}\sum_{k,k',\sigma}\sum_{a,b=L,R}\left[\alpha(\xi_k+\xi_{k'})/2 + \gamma B'\sigma\right] a^\dagger_{k\sigma} b_{k'\sigma}. \tag{8.68}$$

This leads to four different processes, which can be depicted diagrammatically as

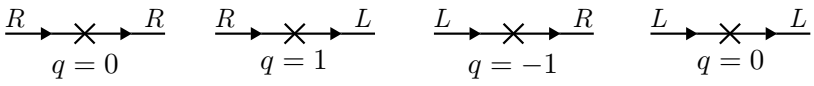

where q denotes the number of particles transferred in the backscattering channel. Evidently, only processes with $q \neq 0$ contribute to the backscattering current. Assuming a

[8] We emphasize that the $\psi_{k\sigma}$ states denote *scattering* states with incoming wave vector k. They are *not* momentum eigenstates and hence involve both left-moving and right-moving contributions.

positive bias (i.e. $\mu_L = eV/2 > \mu_R = -eV/2$), the $T = 0$ rate for the $q = 1$ process is given by

$$\begin{aligned}\Gamma_\alpha &= \frac{2\pi}{\hbar}\sum_{k,k',\sigma}\left|\langle \mathrm{gs}|R^\dagger_{k'\sigma}L_{k\sigma}H_{\mathrm{el}}|\mathrm{gs}\rangle\right|^2 f_L(\xi_{k'})[1-f_R(\xi_k)]\delta(\xi_k-\xi_{k'}) \qquad (8.69)\\ &= \frac{2\pi}{\hbar}\left(\frac{1}{2\pi\rho\, T_K}\right)^2\sum_\sigma \rho^2\int d\epsilon\, f_L(\epsilon)[1-f_R(\epsilon)]\left(\alpha\epsilon+\gamma B'\sigma\right)^2\\ &= \frac{2eV}{h}\left[\frac{\alpha^2}{12}\left(\frac{eV}{T_K}\right)^2+\left(\frac{\gamma B'}{T_K}\right)^2\right],\end{aligned}$$

resulting in a backscattering contribution $I_\alpha = e\Gamma_\alpha$. Here, $|\,\mathrm{gs}\,\rangle$ denotes the ground state of the system. It is easy to verify that the $q = -1$ process has zero phase space for positive bias, and consequently vanishes.

Inelastic backscattering contributions

In a similar fashion, we analyze the inelastic backscattering generated by

$$H_{\mathrm{in}} = \frac{\beta}{4\pi\rho^2 T_K}\sum_{k_1,k_2,k_3,k_4}\sum_{a,b,c,d=L,R} a^\dagger_{k_1\uparrow}b_{k_2\uparrow}c^\dagger_{k_3\downarrow}d_{k_4\downarrow}. \qquad (8.70)$$

This gives rise to $2^4 = 16$ distinct processes, which we evaluate in detail in Appendix L. It is crucial to note that H_{in} allows for the backscattering of *two* right-movers, and the increased phase space results in enhanced rates as compared to single-particle backscattering. In total, the inelastic contributions amount to a backscattering current

$$I_\beta = I_{\beta 1} + I_{\beta 2} = \frac{2e^2}{h}V\frac{5}{12}\beta^2(eV/T_K)^2. \qquad (8.71)$$

Upon summation of these contributions, the total current for the positive-U Anderson model with local Zeeman field is obtained as

$$I = I_u - I_b = \frac{2e^2}{h}V\left[1-(\gamma B'/T_K)^2-\frac{\alpha^2+5\beta^2}{12}\left(\frac{V}{T_K}\right)^2\right]. \qquad (8.72)$$

Due to the onset of backscattering at finite energies, the current is *reduced* with increasing bias voltage. The breaking of spin-symmetry by the local Zeeman field leads to an additional reduction $\sim (B')^2$, as required by symmetry.

Finally, we return to the charge-Kondo effect in the negative-U model by applying the PHLR transformation. The resulting current close to the unitary limit is given by

$$I = I_u - I_b = \frac{2e^2}{h}V\left[1-(\gamma[2\varepsilon_d+U]/T_K)^2-\frac{\alpha^2+5\beta^2}{12}\left(\frac{V}{T_K}\right)^2\right], \qquad (8.73)$$

revealing the current reduction due to a gate detuning from the charge degeneracy point.

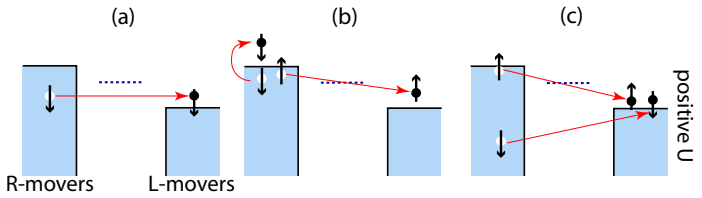

Figure 8.10: Transport processes near the unitary limit for the conventional spin-Kondo effect. The two reservoirs correspond to right-movers (originating from the left lead), and left-movers (originating from the right lead). (a) Elastic backscattering of one right-mover. (b) Inelastic backscattering of one right-mover accompanied by creation of a particle-hole pair within one reservoir. (c) Inelastic backscattering of two right-movers with opposite spins.

8.9.3 Shot noise

In this subsection, we turn to the current shot noise in the Kondo regime. The PHLR transformation allows us to transfer our central results for the conventional Anderson model to the negative-U model. As demonstrated in the previous subsection, close to $T = 0$ and for small bias voltages, the current is nearly unitary, and backscattering events are rare. In this scenario, a sensible definition of the Fano factor does not involve the direct current (which would yield $F = 1$ with small corrections), but rather the backscattering current I_b,

$$F = S/2e|I_b|. \tag{8.74}$$

We have shown, that the backscattering current displays a competition between single-particle backscattering processes, and pair backscattering. Specifically, the relevant processes are

(i) elastic backscattering [$\propto \alpha$, see Fig. 8.10(a)],

(ii) inelastic backscattering of one electron accompanied by creation of a particle-hole pair of either left or right movers [$\propto \beta$, see Fig. 8.10(b)], and

(iii) inelastic backscattering of two rightmovers [$\propto \beta$, see Fig. 8.10(c)].

Since backscattering remains a weak perturbation and events are rare, consecutive backscattering processes will be uncorrelated. Consequently, the zero-frequency noise is obtained as

$$S = 2e(I_\alpha^{(\mathrm{i})} + I_\beta^{(\mathrm{ii})} + 2I_\beta^{(\mathrm{iii})}), \tag{8.75}$$

where roman numbers identify the aforementioned process types. The additional factor of 2 for process (iii) takes into account that the charge of the backscattered pair should enter the noise quadratically. As a result, the Fano factor is given by

$$F = \frac{2(B'/T_K)^2 + \frac{5}{3}(V/T_K)^2}{2(B'/T_K)^2 + (V/T_K)^2}. \tag{8.76}$$

(Here, we have exploited the identity of the coefficients α, β, and γ, which follows from comparison with the Bethe ansatz [136].) Remarkably, for vanishing local Zeeman field,

Eq. (8.76) leads to a super-Poissonian Fano factor $F = 5/3$ due to pair backscattering. It is the enhanced phase space for pair scattering which renders its contribution dominant, despite the fact that it constitutes only one of the seven relevant processes. In the opposite limit of large Zeeman fields $B' \gg V$, single-particle backscattering at the singlet dominates and the Fano factor is Poissonian, $F = 1$.

A straightforward application of the PHLR mapping now yields the corresponding Fano factor for the negative-U model,

$$F = \frac{2([2\varepsilon_d + U]/T_K)^2 + \frac{5}{3}(V/T_K)^2}{2([2\varepsilon_d + U]/T_K)^2 + (V/T_K)^2}. \tag{8.77}$$

Interestingly, the fragility of the charge-Kondo effect is also directly reflected in the current shot noise: The Fano-factor enhancement only dominates the immediate vicinity of the charge-degeneracy point. A detuning from this point results in a suppression of the Fano factor, and Poissonian noise is recovered as soon as the detuning is large compared to the bias voltage.

8.10 Extension: Breaking of the LR symmetry

We finally comment on the consequences of LR-symmetry breaking. In particular, we consider the case of symmetric voltage splitting [the splitting ratio is fixed by the capacitance ratio of the junctions], but broken left-right symmetry regarding the couplings, i.e. $t_L \neq t_R$. The PH transformation is not affected by the coupling asymmetry, so that its general result is given by Eq. (8.33). By contrast, the LR transformation crucially depends on the left-right symmetry. Breaking this symmetry results in a mapping to the following positive-U model,

$$\begin{aligned} H' = &\frac{U}{2}\sum_\sigma n'_{d\sigma} - U n'_{d\uparrow} n'_{d\downarrow} + \sum_{ak\sigma} (\epsilon_{ak} - aeV/2) n'_{ak\sigma} \\ &+ \sum_{ak\sigma} \left(t'_{ak\sigma} c'^\dagger_{ak\sigma} d'_\sigma + \text{h.c.} \right) + (\varepsilon_d + U/2)(n'_{d\uparrow} - n'_{d\downarrow}), \end{aligned} \tag{8.78}$$

where

$$t'_{ak\uparrow} = t_{ak}, \quad t'_{Lk\downarrow} = t_{Rk}, \quad t'_{Rk\downarrow} = t_{Lk}. \tag{8.79}$$

Accordingly, transport in the negative-U model with asymmetric coupling is equivalent to transport in a positive-U model with local Zeeman field and *spin-dependent* tunneling matrix elements. Specifically, for one spin direction (here: $\uparrow$) the couplings are Γ_L and Γ_R for the left and right junction, respectively. For the other spin direction ($\downarrow$) however, the couplings are interchanged and are Γ_R (Γ_L) in the left (right) junction.[9]

[9] We note that this is consistent with the independence of the linear conductance on LR symmetry, as the system only couples to the symmetric combination of the left and right lead in linear response (Glazman-Raikh transformation). In fact, in combination with the Glazman-Raikh transformation, Eq. (8.78) can be used for a second independent proof of the identity of conductances in the negative-U and the corresponding positive-U model.

8.11 Conclusions

Near the degeneracy point, transport through a molecular junction with negative U differs drastically from the conventional Coulomb-blockade scenario at positive U. At high temperatures $T \gg T_K$, negative U results in current flow making the molecule alternate in time between even occupation numbers. This is accomplished by pair tunneling, which is the dominant transport mode in the gate-voltage – bias-voltage domain shown in Fig. 8.4.

It is intriguing that the on-site attraction of two electrons makes pair tunneling through molecules qualitatively similar to tunneling through a superconducting grain, considered in Ref. [137]. However, in the case of molecules, the physical picture of transport is more complex. This is because a pair can be created on the molecule by electrons tunneling from *different* leads, as illustrated in Fig. 8.1(d). By contrast, for a grain with size larger than the superconducting correlation length, electron pairs enter and exit the grain only from the *same* lead, i.e. only the processes in Fig. 8.1(c) are responsible for the passage of current.[10] As an important consequence of this difference, negative-U molecules act as gate-controlled rectifiers. Apart from these characteristic fingerprints in current-voltage characteristics, the pair-induced correlations also lead to super-Poissonian shot noise, which are most prominent for roughly symmetric devices.

The PHLR transformation, developed for mapping transport in negative-U molecules to transport through conventional positive-U centers with a local Zeeman field, has proven to be a valuable tool in deepening our understanding of both negative-U and positive-U transport scenarios. In particular, it has served as a key ingredient in our investigation of the charge-Kondo regime. Our results for the linear conductance and the nonlinear IV analytically confirm the fragility of the charge-Kondo effect: Any gate-voltage detuning from the charge-degeneracy point results in a departure from the unitary limit, which is in contrast to the conventional spin-Kondo effect. Remarkably, we find that backscattering of electron pairs also plays an important role deep inside the Kondo regime, and leads to super-Poissonian noise in the backscattering current with Fano factor $F = 5/3$ at the degeneracy point.

[10] Another difference between transport through negative-U molecules and superconducting grains lies in the absence of BCS coherence factors in the former.